

Experimental realization of an entanglement filter through the environmental selection

C. Zu¹, Y.-X. Wang¹, X.-Y. Chang¹, P.-Y. Hou¹, H.-X. Yang¹, L.-M. Duan^{1,2}
¹*Center for Quantum Information, IIIS, Tsinghua University, Beijing, China and*
²*Department of Physics, University of Michigan, Ann Arbor, Michigan 48109, USA*

We report an experiment that uses the environmental selection, a key concept in the recent theory of quantum Darwinism, as a mechanism to realize the entanglement filter, a useful quantum information device that filters out certain entangled states. In the experiment, the environment of two qubits is controlled to favor an entangled state and kill other competing components in the input state. The initial state has vanishing entanglement, but the state surviving after interaction with the environment is close to a maximally entangled state, with an entanglement fidelity of $(94.7 \pm 1.9)\%$ measured through the quantum state tomography. We experimentally demonstrate that the generated entanglement is robust under change of the initial state configurations and the environmental parameters.

PACS numbers:

Environmental selection, a key concept in Darwin's theory of evolution, has found important applications in several areas of science. A striking example in quantum physics is the mechanism known as quantum Darwinism, recently proposed to explain the emergence of classical reality from the quantum world [1–5]. The concept of quantum Darwinism has found interesting applications in theory of quantum measurements [1–5]. In quantum measurement process, the fittest states selected out by the environment correspond to the classical pointer states [1, 2]. The state of the system, originally in a quantum superposition, tends to collapse onto the pointer states due to the environmental interaction. The proliferation of the classical pointer states in the environment explains their robustness and the appearance of a classical reality through the measurement, but at the same time it induces decoherence in the system, reducing its potential for quantum information. [1, 2].

With advance of quantum control techniques [6], it becomes possible to engineer the environment of quantum systems in such a way that the fittest state selected out by the environment corresponds to a quantum entangled state. The environmental selection, a key concept in quantum Darwinism, can then be used in a novel way as a mechanism to realize an entanglement filter. Just like a polarization filter which can select out certain polarization states, the entanglement filter is a useful quantum information device proposed in Refs. [7, 8] to filter out certain entanglement components. An entanglement filter that can select out two-qubit states according to the parity of their polarizations has been realized recently [8].

In this paper, we report an experiment that demonstrates a new type of entanglement filter based on the mechanism of the environmental selection. This entanglement filter selects out a certain entangled Bell state, which corresponds to the fittest state in a specially designed environment for two propagating photonic qubits. Through the environmental selection, the entan-

glement filter generates almost maximally entangled output state with a measured entanglement fidelity about $(94.7 \pm 1.9)\%$ from the unentangled input states. Note that the environmental coupling is typically in favor of classical states and leads to decay of quantum entanglement. Dissipation from the environmental coupling has been generally identified as the major obstacle for realization of quantum information processing. There are striking exceptions where controlled dissipation under certain configurations become helpful for entanglement generation [9–14]. Our reported experiment belongs to this striking class, where the environmental selection emerging from the dissipation is used as a mechanism to realize an entanglement filter, which generates entanglement from unentangled input states.

In our experiment, the input state is a mixture of two classical states

$$\rho_{in} = |c_0|^2 |HV\rangle\langle HV| + |c_1|^2 |VH\rangle\langle VH| \quad (1)$$

with arbitrary mixing coefficients $|c_0|^2$ and $|c_1|^2$, where $|H\rangle$ ($|V\rangle$) represents a single-photon state with horizontal (or vertical) polarization. The input state ρ_{in} is in a two-dimensional subspace spanned by $|HV\rangle$ and $|VH\rangle$. Alternatively, we can take the Bell states $|\Psi^\pm\rangle = (|HV\rangle \pm |VH\rangle)/\sqrt{2}$ as the basis-vectors for this subspace. Using $|\Psi^\pm\rangle$ as the basis-vectors, the state ρ_{in} is expressed as $\rho_{in} = (|\Psi^+\rangle\langle\Psi^+| + |\Psi^-\rangle\langle\Psi^-|)/2 + (|c_0|^2 - |c_1|^2)(|\Psi^+\rangle\langle\Psi^-| + |\Psi^-\rangle\langle\Psi^+|)$. We design an environment so that it favors a certain entangled state, say $|\Psi^+\rangle$, and leads to large decay of the other component ($|\Psi^-\rangle$ in this case) with a decay ratio $\beta = e^{-\gamma_-}/e^{-\gamma_+} < 1$. This realizes an entanglement filter that selects out the $|\Psi^+\rangle$ state. After the environment, the effective output state (unnormalized) has the form

$$\begin{aligned} \rho_{out} = & (|\Psi^+\rangle\langle\Psi^+| + \beta|\Psi^-\rangle\langle\Psi^-|)/2 \\ & + (|c_0|^2 - |c_1|^2)\sqrt{\beta}(|\Psi^+\rangle\langle\Psi^-| + |\Psi^-\rangle\langle\Psi^+|) \end{aligned}$$

In the limit with $\beta \ll 1$, the output state becomes maximally entangled although the input state ρ_{in} apparently has no entanglement. In the simple case of $|c_0|^2 = |c_1|^2$, the entanglement of ρ_{out} , measured by the concurrence C [15], has the analytic form $C = (1 - \beta) / (1 + \beta)$.

To experimentally produce the mixed state in the form of Eq. (1) for two photons, we generate the photon pair through the spontaneous parametric down conversion (SPDC) in a nonlinear BBO crystal. The experimental setup is shown in Fig. 1. The pumping pulse before the BBO crystal is in the polarization state $c_0 |H\rangle + c_1 |V\rangle$, where the ratio c_0/c_1 is set by the angle of a half wave plate (HWP). After the BBO crystal, the down converted photons are in the state $|\Psi\rangle = c_0 |H, f_H(t)\rangle |H, f_H(t)\rangle + c_1 |V, f_V(t)\rangle |V, f_V(t)\rangle$, where $|f_H(t)\rangle$ ($|f_V(t)\rangle$) denotes the pulse shape of the corresponding photon with horizontal (vertical) polarization. Due to the birefringence in the BBO crystal, the shape functions $f_H(t)$ and $f_V(t)$ for different polarization components do not perfectly overlap in time. To generate entanglement, typically we need another birefringent crystal, such as a quartz, to compensate this mismatch in the pulse shapes. In this experiment, we set the quartz compensator in the reserve direction, so the shape mismatch of the pulses is actually amplified. As a result, we have $\langle f_H(t) | f_V(t) \rangle \approx 0$, and the polarization state of the down converted photons, after tracing over the shape degrees of freedom, is described by the mixed state $|c_0|^2 |HH\rangle \langle HH| + |c_1|^2 |VV\rangle \langle VV|$. After another HWP which exchanges the states $|H\rangle$ and $|V\rangle$ for one of the photons, we get a state in the form of ρ_{in} described by Eq. (1).

To experimentally confirm that the input state to the optical channel has vanishing entanglement, we perform quantum state tomography on the state ρ_{in} . For two-qubit states, the quantum state tomography is done with 16 independent measurements in complementary bases and the density matrix is reconstructed using the maximum likelihood method [16]. The density matrix from the experimental measurement is shown in Fig. 2 when $c_0 = c_1 = 1/\sqrt{2}$. The data is consistent with the state $\rho_{in} = (|HV\rangle \langle HV| + |VH\rangle \langle VH|)/2$ with small off-diagonal matrix elements. The off-diagonal matrix elements result from the small but non-zero overlap between the pulse shapes $f_H(t)$ and $f_V(t)$ for the horizontal and the vertical polarization components. From the measured density matrix, the concurrence for the input state is found to be $C = 0.040 \pm 0.024$, which indicates that the entanglement for input state is close to zero. The error bars in C and other experimentally measured quantities account for the statistical error associated with the photon detection under the assumption of a Poissonian distribution for the photon counts.

Now the input state goes through an entanglement filter represented by the optical channel shown in Fig. 1 which has a tunable environmental coupling induced by

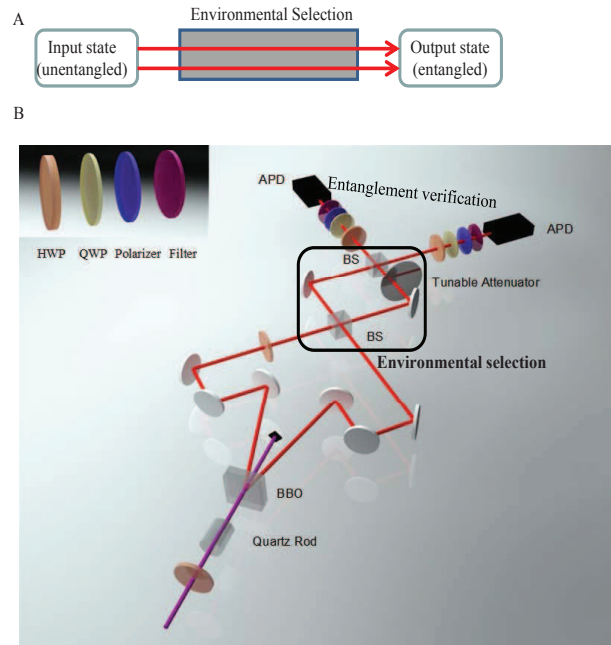


FIG. 1: (A) Illustration of an entanglement filter through the environmental selection. (B) Experimental setup that realizes an entanglement filter through the environmental selection. Before the box, a spontaneous parametric down conversion process prepares two single photons in unentangled states. Ultrafast laser pulses (with the pulse duration less than 150 fs and a repetition rate of 76 MHz) at the wavelength of 400 nm from a frequency doubled Ti:sapphire laser pump two joint beta-barium-borate (BBO) crystals, each of 0.6 mm depth with perpendicular optical axis, to generate photon pairs at the wavelength of 800 nm. Birefringent quartz crystals induce large shape mismatch between horizontal and vertical polarization components of the pulses, and the input state to the box thus has vanishing entanglement as verified by quantum state tomography. The setup inside the box realizes an entanglement filter through a dissipative optical channel (environment) which selects out one of the maximally entangled Bell states as the fitted state from this environment. After the box, the entanglement is verified through quantum state tomography, using wave plates, single-photon detectors, and coincidence measurements.

an attenuator. The attenuator, together with the Hong-Ou-Mandel interference setup in Fig.1, introduces different decay rates for the Bell states $|\Psi^+\rangle$ and $|\Psi^-\rangle$. After the first beam splitter in Fig.1, the two photons will go along the same path (with 1/2 probability for each path) if they are in the state $|\Psi^+\rangle$ and different paths if they are in $|\Psi^-\rangle$. An attenuator induces loss of photons in one of the paths with the attenuation factor $e^{-\gamma}$. So the net attenuation factors for the state $|\Psi^+\rangle$ and $|\Psi^-\rangle$ are given respectively by $(1 + e^{-2\gamma})/2$ and $e^{-\gamma}$. Apparently, the state $|\Psi^+\rangle$ has a smaller attenuation in this optical channel. So, the environment favors the entangled state $|\Psi^+\rangle$ by killing its competing component $|\Psi^-\rangle$

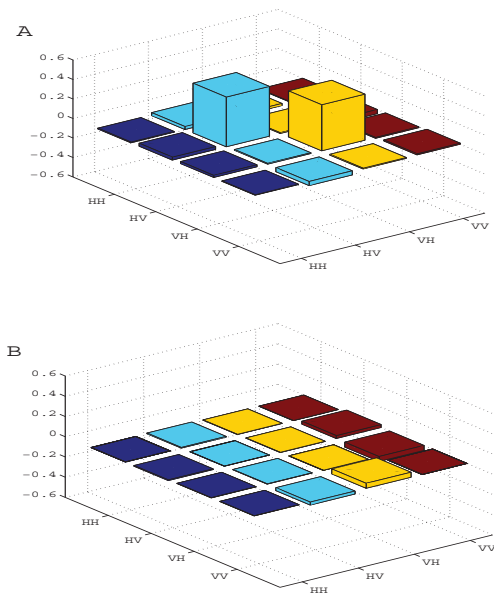


FIG. 2: Real (A) and imaginary (B) parts of the density matrix of the input state to the environment reconstructed through the quantum state tomography.

at a faster rate. After this optical channel, the emerging photons after the second beam splitter is described by the effective state ρ_{out} in the form of Eq. (2) with the decay ratio $\beta = 2/(e^{-\gamma} + e^{\gamma})$ (Note that similar to other SPDC experiments, the vacuum components at any output port of the optical channel are dropped as they will be erased by the single-photon detection and coincidence measurement). The concurrence of ρ_{out} is then given by $C = \tanh^2(\gamma/2)$, which approaches to the unity corresponding to a maximally entangled state when the attenuation factor $e^{-\gamma} \ll 1$.

To verify entanglement generated by the entanglement filter through the environmental selection, we perform quantum state tomography on the output state ρ_{out} . Figure 3 shows the elements of the density matrix reconstructed from the experimental data. The output ρ_{out} is pretty close to a pure state with the density matrix $|\Psi_{\theta}\rangle\langle\Psi_{\theta}|$, where $|\Psi_{\theta}\rangle = (|HV\rangle + e^{i\theta}|VH\rangle)/\sqrt{2}$ with $\theta \approx 0.150\pi$. The state deviates by a relative phase shift θ from the survivor state $|\Psi^+\rangle$ that one expects from the above analysis. The reason for this deviation is that the beam splitter in our setup has birefringence, which induces slightly different relative phases for the horizontal and the vertical polarization components on the output paths (see the characterization in the method section). Note that θ is just a fixed phase shift which can be easily compensated with no influence on entanglement. From the measured density matrix ρ_{out} , the entanglement fidelity for the output state, defined as the overlap of ρ_{out} with the closest maximally entangled state, is found to be $F_e = 0.947 \pm 0.019$. A bound on the entanglement fidelity

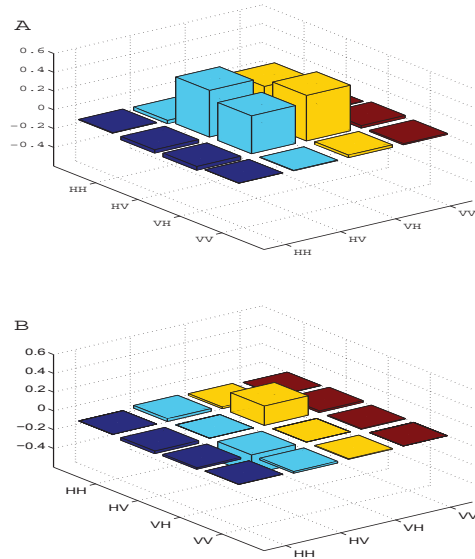


FIG. 3: Real (A) and imaginary (B) parts of the density matrix of the output state after the environmental selection reconstructed through the quantum state tomography.

with $F_e > 1/2$ is a witness for entanglement [17]. From the measured matrix elements, the concurrence for the state ρ_{out} is calculated, given by $C(\rho_{out}) = 0.902 \pm 0.028$, which suggests that substantial entanglement has been generated in our experiment through the environmental selection.

To confirm that the environmental selection is the mechanism for entanglement generation, we control the survival probabilities for the states $|\Psi^+\rangle$ and $|\Psi^-\rangle$ in the optical channel by tuning the attenuation γ and measure how the entanglement varies under change of the environmental selection strength (which corresponds to a partial entanglement filter). For each case, the output state of the optical channel is reconstructed experimentally through the quantum state tomography and its entanglement is directly calculated from the measured density matrices. In Fig. 4, we show the measured entanglement in term of concurrence for the output state under different loss rate $\epsilon = 1 - e^{-\gamma}$, and the results are compared with the theoretical prediction based on the environmental selection. With a small loss rate ϵ , which corresponds to the case of weak environmental selection, the entanglement is tiny. As the strength of the environmental selection increases by tuning up the loss ϵ , entanglement significantly increases and eventually approaches the unity when $\epsilon \rightarrow 1$. The agreement between the data and the theoretical prediction within the uncertainty imposed by the experimental imperfection indicates that the environmental selection is the underlying mechanism for entanglement generation.

The entanglement generated from the environmental

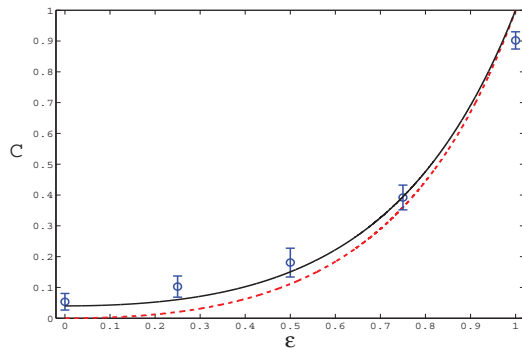


FIG. 4: The entanglement (in concurrence C) of the output state as a function of the loss rate ϵ induced by the attenuator. The density matrices are reconstructed at each data point through the quantum state tomography, and the entanglement is calculated from the experimentally measured density matrices, with the error bar coming from the statistical error in photon counts. The solid (dashed) lines are from theoretical predictions based on the environmental selection mechanism. We use the ideal input state in Eq. (1) with $|c_0|^2 = 1/2$ for the dashed line (where $C = \tanh^2(\gamma/2) = \epsilon^2/(2-\epsilon)^2$) and the real input state reconstructed in Fig. 2 through quantum state tomography for the solid line.

selection is robust under change of various experimental parameters or configurations, as shown in Table 1. First, it is insensitive to the initial state. We arbitrarily rotate the polarization of the pumping laser through a half wave plate, and entanglement of the output state remains basically unchanged within the experimental error bar. For instance, when the pumping pulse is set to horizontal polarization, the input state to the optical channel becomes $|HV\rangle$ (apparently unentangled), which can be written as a superposition of $|\Psi^+\rangle$ and $|\Psi^-\rangle$ states. As the $|\Psi^-\rangle$ component is diminished by the environmental selection, the output state becomes a maximally entangled one. The measured concurrence in this case is 0.902 ± 0.020 . Second, the entanglement generation here is also insensitive to some environmental parameters. For instance, if we insert a quarter wave plate to change the relative phase between the two arms of the optical channel in the box of Fig. 1, the change to the measured concurrence shown in Table 1 is tiny and within the experimental error bar. Finally, note that in the conventional SPDC setup, the pulse shape compensation is a critical requirement for entanglement generation. Here, when the entanglement is generated by the environmental selection, we do not need any shape compensation after or before the BBO crystal. If we remove the birefringent quartz crystals or add more of them in Fig. 1, the variation of the entanglement fidelity and the concurrence remains negligible as shown in Table 1.

Configurations	Entanglement fidelity	Concurrence
case I	0.947 ± 0.019	0.902 ± 0.028
case II	0.940 ± 0.012	0.902 ± 0.020
case III	0.934 ± 0.014	0.897 ± 0.026
case IV	0.952 ± 0.013	0.923 ± 0.026

Table 1: Entanglement fidelity and concurrence of the output state after the environmental selection under different configurations of the input state and environment. Case I corresponds to a mixed input state to the environment where the density matrix is shown in Fig. 2. In case II, the polarization of the pumping laser is in horizontal direction, corresponding to a product input state $|HV\rangle$ to the environment. In case III, we insert a quarter wave plate in one arm of the optical channel, which induces a relative phase shift between the two polarization components. In case IV, we remove one quartz crystal which changes the shape mismatching for the polarization components in the input state.

In this paper, we report an experiment that demonstrates a new type of entanglement filter based on the environmental selection, a key concept in the recent theory of quantum Darwinism. We have experimentally confirmed that the entanglement filter generates high-fidelity entangled states through selection-out of the fittest component from the initially unentangled states. The entanglement filter may prove to be a useful quantum information device, with its ability to robustly generate and manipulate entanglement.

Appendix: Birefringence of the beam splitter

A balanced non-polarizing beam splitter induces a transformation $a_1 \rightarrow (a_1 + a_2)/\sqrt{2}$, $a_2 \rightarrow (a_2 - a_1)/\sqrt{2}$ to its input-output modes for both the horizontal ($a = h$) and the vertical ($a = v$) polarization components. However, the beam splitters used in our experiment have a small birefringence where the transformation can be represented by $h_1 \rightarrow (h_1 + h_2)/\sqrt{2}$ and $v_1 \rightarrow (v_1 e^{i\theta_1} + v_2 e^{i\theta_2})/\sqrt{2}$. Compared with the conventional transformation, we should replace $|V_1\rangle$ and $|V_2\rangle$ with $|V_1\rangle e^{i\theta_1}$ and $|V_2\rangle e^{i\theta_2}$, and the fittest state selected out by the environment thus becomes $|\Psi_\theta\rangle = (|HV\rangle + e^{i\theta} |VH\rangle)/\sqrt{2}$ with $\theta = \theta_1 - \theta_2$. Using a laser beam at 800 nm wavelength, we measure the angles θ_1 and θ_2 by setting the input at the polarization state $(|H\rangle + |V\rangle)/\sqrt{2}$ and find that $\theta_1 = 7.2^\circ$ and $\theta_2 = -18.6^\circ$ for our beam splitter, which gives $\theta = 25.8^\circ \simeq 0.143\pi$, in good agreement with the state in Fig. 3 reconstructed from the quantum state tomography.

Acknowledgement This work was supported by the National Basic Research Program of China (973 Program) 2011CBA00300 (2011CBA00302) and the NSFC Grant 61033001. LMD acknowledges in addition support from the IARPA MUSIQ program, the ARO and the AFOSR MURI program.

-
- [1] W. H. Zurek, *Rev. Mod. Phys.* 75, 715 (2003).
[2] W. H. Zurek, *Nature Phys.* 5, 181 (2009).
[3] S. Lloyd, *Nature Phys.* 5, 164 (2009).
[4] H. Ollivier, D. Poulin, W. H. Zurek, *Phys. Rev. Lett.* 93, 220401 (2004).
[5] R. Blume-Kohout, W. H. Zurek, *Phys. Rev. Lett.* 101, 240405 (2008).
[6] C. Monroe, *Nature* 416, 238 (2002).
[7] H. F. Hofmann, S. Takeuchi, *Phys. Rev. Lett.* 88, 147901 (2002).
[8] R. Okamoto et al., *Science* 323, 483 (2009).
[9] L.-M. Duan, M. Lukin, J. I. Cirac, P. Zoller, *Nature* 414, 413 (2001).
[10] D. L. Moehring et al., *Nature* 449, 68 (2007).
[11] S. Diehl et al., *Nature Physics* 4, 878-883 (2008).
[12] F. Verstraete, M. M. Wolf, J. I. Cirac, *Nature Physics* 5, 633 (2009).
[13] H. Krauter et al., *Phys. Rev. Lett.* 107, 080503 (2011).
[14] F. Bariani, Y. O. Dudin, T. A. B. Kennedy, A. Kuzmich, *Phys. Rev. Lett.* 108, 030501 (2012).
[15] W. K. Wootters, *Phys. Rev. Lett.* 80, 2245 (1998).
[16] D. F. V. James et al., *Phys. Rev. A* 64, 052312 (2001).
[17] B. B. Blinov, D. L. Moehring, L. M. Duan, C. Monroe, *Nature* 428, 153 (2004).